THE JOURNAL OF PHYSICAL CHEMISTRY Letters

Letter

pubs.acs.org/JPCL

# Theoretical Model of Oxidative Adsorption of Water on a Highly Reduced Reconstructed Oxide Surface

Nathan Z. Koocher, John Mark P. Martirez, and Andrew M. Rappe*

The Makineni Theoretical Laboratories, Department of Chemistry, University of Pennsylvania, Philadelphia, Pennsylvania 19104-6323 United States

Supporting Information

**ABSTRACT:** Highly reduced surface reconstructions of $BaTiO_3$ (001) have been found to be composed of a $TiO_2$ surface covered with Ti adatoms occupying surface interstitial sites. We predict the reactivity of these highly oxophilic and reduced surface Ti species through density functional theory, where we calculate the adsorption of $H_2O$ on the $(\sqrt{5} \times \sqrt{5})R26.6°$ $TiO_2$–$Ti_{3/5}$ reconstruction. $H_2O$ serves as the primary O source and oxidizing agent. We demonstrate that $H_2O$ oxidizes some of the Ti adatoms, shifting their occupied 3d states to the surface conduction band edge. We find that, due to the high concentration of reduced Ti species on the surface, a dissociative adsorption of water on the reconstructed surface can also lead to the formation of surface hydrides, which serve as a precursor for $H_2$ evolution. This suggests that the reconstructed surface may be an attractive single-phase hydrogen evolution catalyst.

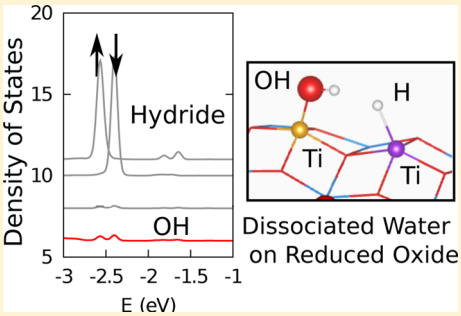


**SECTION:** Surfaces, Interfaces, Porous Materials, and Catalysis

Water can interact with surfaces in many ways. For example, on metallic surfaces, water can form an ordered monolayer upon adsorption (physical adsorption);[1−3] on metal oxide surfaces, water can simultaneously hydroxylate and protonate a surface (chemisorption, acid−base reaction)[4] or can act as an oxidizing agent, for example, by filling surface oxygen vacancies (redox reaction).[5] Interaction of metal oxides with water has been, and still is, of great interest due to the diversity of applications of this type of compound, from electronics to sensing devices to catalysis, where water directly or indirectly contributes to the demise or success of a device.[6−9]

With recent advances in material synthesis and surface structure manipulation, interesting surface structures with little known or unknown chemistry have been created and identified. Among the particularly well studied oxides is the perovskite family. Two types of theoretical studies populate the literature of water interacting with perovskite-type oxide surfaces: those that deal with ideal surfaces and those that deal with reconstructed surfaces. Of the surfaces surveyed, emphasis is placed on $SrTiO_3$ (STO), with fewer studies addressing $BaTiO_3$ (BTO). To the best of our knowledge, furthermore, there are no reports of surface reconstructions of BTO interacting with water. Regarding STO surfaces, molecular and dissociative adsorption to the perfect surface (both SrO and $TiO_2$ terminations) has been modeled.[10−12] More recently, reconstructed STO surfaces have also been investigated.[13−16] Regarding BTO surfaces, it was recently found that water dissociatively adsorbs on the BTO (001) surface.[17] $H_2O$ was also found to reverse the surface layer buckling on the (001) surface of BTO,[8,6] whereas surface hydroxyls were found to stabilize out-of-plane polarization in BTO nanowires due to its effective positive polarization charge screening.[18] Despite these studies, the reactivity of BTO surface reconstructions has not been examined.

$BaTiO_3$, a prototypical perovskite, has been shown to exhibit various surface reconstructions in reducing environments.[19−21] These reconstructions are Ti-enriched surfaces, where surface reduction is achieved not exclusively through formation of surface O vacancies but also through excess surface Ti adatoms[19,20] or TiO ad-units,[21] analogous to Ti interstitials in bulk. One particular example is the $(\sqrt{5} \times \sqrt{5})R26.6°$ reconstruction of $BaTiO_3$ (001) surface, the structure of which has been characterized as having a Ti adatom coverage of three-fifths, four-fifths, or some combination of the two on a $TiO_2$ termination.[20]

Here, we report the effect of water adsorption on the aforementioned $(\sqrt{5} \times \sqrt{5})R26.6°$ $BaTiO_3$ surface reconstruction. Through density functional theory (DFT), we demonstrate enhanced water reactivity of a metal oxide due to a surface reconstruction enabling adsorption channels that are otherwise inaccessible on the bulk-like stoichiometric surface. These adsorption channels lead to formation of stable surface hydrides that may be used to do various useful reductive chemistries. The dual nature of the surface investigated offers both a Lewis acid site for the usual water dissociation and a redox active site for hydride formation. This is a quality that is

**Received:** August 4, 2014
**Accepted:** September 10, 2014

   dx.doi.org/10.1021/jz501635f | J. Phys. Chem. Lett. 2014, 5, 3408−3414

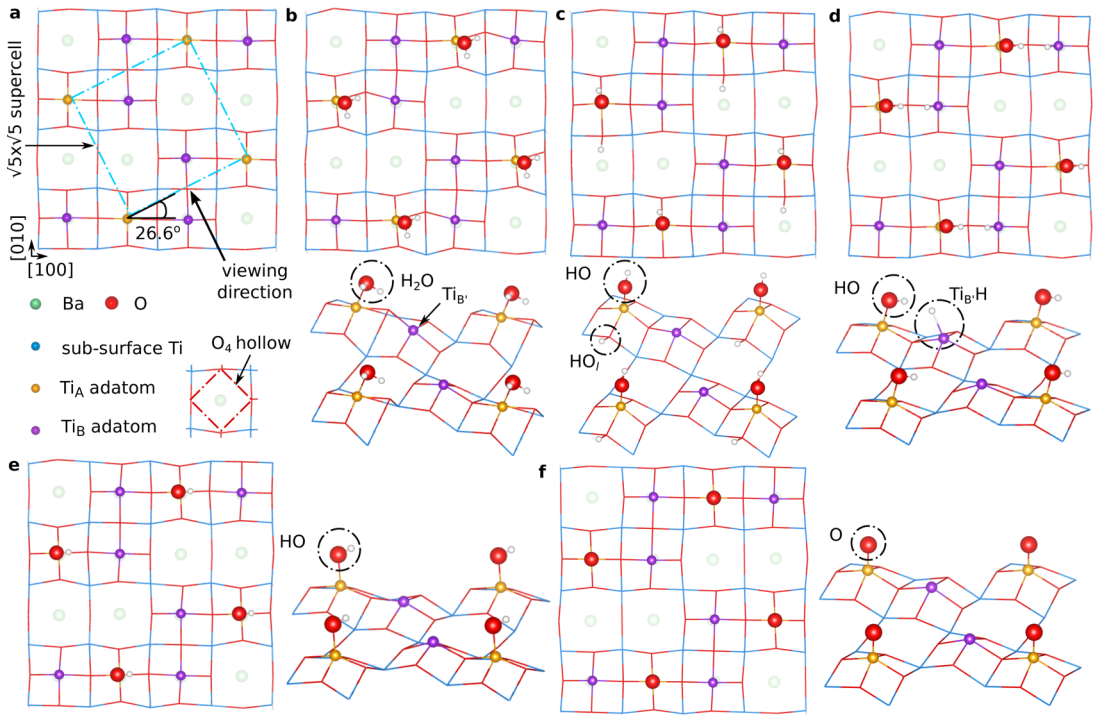


**Figure 1.** Different adsorption products of a water molecule on the Ti adatom rich reconstruction of $BaTiO_3$. (a) Bare $(\sqrt{5} \times \sqrt{5})R26.6°$ $TiO_2$−$Ti_{3/5}$ reconstruction (based on ref 20), showing 4-fold coordinated Ti adatoms ($Ti_A$ and $Ti_B$) on the $TiO_2$ (001) termination. (b)−(f) different adsorption products of $H_2O$ on $Ti_A$: (b) molecular; (c) dissociative with H on a lattice O ($O_l$); (d) dissociative with H on $Ti_{B'}$; (e) oxidative with surface OH as the product; and (f) oxidative with surface O as the product. Viewing direction for the angled-view structures is shown in (a).

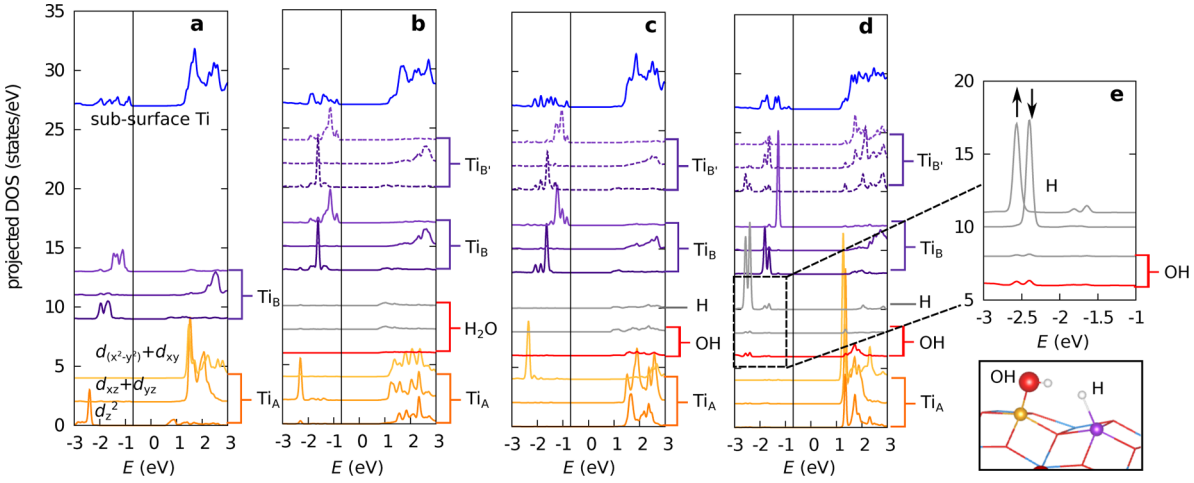


**Figure 2.** Electronic PDOS of the adsorption products of a water molecule on the $(\sqrt{5} \times \sqrt{5})R26.6°$ reconstruction.(a) Bare $(\sqrt{5} \times \sqrt{5})R26.6°$ $TiO_2$−$Ti_{3/5}$ reconstruction (based on ref 20). Resulting PDOS after: (b) molecular; (c) dissociative with H on a lattice O ($O_l$); and (d) dissociative with H on $Ti_{B'}$. For Ti adatoms (A and B (B′)), the DOS contribution is resolved to show orbital types: $d_{z^2}$, $d_{xz}$ + $d_{yz}$ and $d_{x^2-y^2}$ + $d_{xy}$ from bottom to top. See Figure 1a−d for the corresponding atomic structures. (e) Spin-resolved 1s orbital projection of the H on $Ti_{B'}$ showing hydride orbital occupation in (d). By contrast, the H in OH does not have occupied 1s orbital (cationic). Lower panel in (e) shows the surface $Ti_A$−OH and the adjacent $Ti_{B'}$−H structure (see Figure 1d for legend). For the PDOS, the valence band maxima were aligned, which are set to −0.7 eV[20] for ease of comparison.

rare for a homogeneous surface. Mechanisms for $H_2$ generation on the reconstructed surface are also presented.

Starting from the reconstructed atomic structure,[20] we explore various water adsorption configurations and coverages, paying particular attention to the interaction of water with the undercoordinated Ti adatoms. Shown in Figure 1a is the $(\sqrt{5} \times \sqrt{5})R26.6°$ $TiO_2$−$Ti_{3/5}$ reconstruction (without $H_2O$). The structure shows two types of Ti adatoms, $Ti_A$ (yellow) and $Ti_B$ (purple) on $O_4$ hollow sites of the $TiO_2$ (001) termination. The Ti adatoms are differentiated according to their Ti-adatom neighbors. $Ti_A$ has two Ti adatom neighbors (two $Ti_B$) along the [100] direction, while $Ti_B$ has its two Ti adatom neighbors ($Ti_A$ and another $Ti_B$) along [001] and [010] directions. These atoms are shown to have different electronic structures, where $Ti_A$ has its $d_{z^2}$ orbital occupied, whereas $Ti_B$ has its $d_{z^2}$, $d_{xy}$, and $d_{x^2-y^2}$ orbitals occupied, indicating that these adatoms are highly reduced.[20] Shown in Figure 2a is the orbital projected density of states (PDOS) of these surfaces. Water can interact with the


dx.doi.org/10.1021/jz501635f | J. Phys. Chem. Lett. 2014, 5, 3408−3414

Table 1. Löwdin Charges[a] of Select Surface Species after Reaction of Water with the $(\sqrt{5} \times \sqrt{5})R26.6°$ $TiO_2$−$Ti_{3/5}$ Reconstruction[b]

| structure | adsorption type | $Ti_A$ | $Ti_B$ | $Ti_{B'}$ | $O_w$ | $H_{hxyl}$ | $H_{diss}$ |
|---|---|---|---|---|---|---|---|
| 1a | none | +2.07 | +1.80 | +1.80 | | | |
| 1b | physisorption | +2.08 | +1.80 | +1.82 | −0.79 | +0.42 | +0.36 |
| 1c | dissociative | +2.12 | +1.79 | +1.79 | −1.01 | +0.41 | +0.39 |
| 1d | dissociative | +2.27 | +1.79 | +2.11 | −0.88 | +0.37 | −0.67 |
| 1e | oxidative | +2.28 | +1.79 | +1.80 | −0.94 | +0.41 | |
| 1f | oxidative | +2.14[c] | +1.79 | +1.79 | −0.87 | | |

[a]In electron charge, *e*. [b]The structures are found in Figure 1. Bulk Ti: +2.33 *e*; bulk O: − 1.02 *e*. $O_w$ is O from water; $H_{hxyl}$ is H in hydroxyl; $H_{diss}$ is H-bonded to a surface O or dissociated H on a lattice O ($O_l$) or $Ti_{B'}$. [c]Less positive due to the very covalent bond between $Ti_A$ and $O_w$, leading also to less negative charge on $O_w$.

surface via molecular, dissociative, or oxidative adsorption. In all cases, the oxygen of the $H_2O$ would bond to either $Ti_A$ or $Ti_B$. When water breaks the symmetry between the two $Ti_B$ adatoms, one will be referred to as B and the other B′. Because the surface is highly reduced, with combined adatomic and sublayer ($TiO_2$) Ti:O ratio of (1 + 3/5):2 = 4:5, we explored physical and dissociative, as well as oxidative adsorption of $H_2O$, described by the following reactions:

$$Ti_{A/B} + H_2O \rightarrow Ti_{A/B}{-}OH_2 \quad (1)$$

$$Ti_{A/B} + O_{lattice} + H_2O \rightarrow Ti_{A/B}{-}OH + O_{lattice}H \quad (2)$$

$$Ti_{A/B} + Ti_{B/A} + H_2O \rightarrow Ti_{A/B}{-}OH + Ti_{B/A}H \quad (3)$$

$$Ti_{A/B} + H_2O \rightarrow Ti_{A/B}{-}OH + \frac{1}{2}H_2 \quad (4)$$

$$Ti_{A/B} + H_2O \rightarrow Ti_{A/B} = O + H_2 \quad (5)$$

$$2Ti_{A/B}{-}OH + Ti_{B/A}H + O_{lattice}H \rightarrow Ti_{B/A} + O_{lattice} + H_2 + 2Ti_{A/B}{-}OH \quad (6)$$

$$Ti_{A/B}{-}OH + Ti_{B/A}H \rightarrow Ti_{A/B} = O + H_2 \quad (7)$$

Reaction 1 describes molecular adsorption, reactions 2 and 3 describe different dissociative adsorption channels, reactions 4 and 5 describe different oxidative adsorption channels (which will be further discussed below), and reactions 6 and 7 describe required reactions for $H_2$ evolution. We model low coverage situations where a single adsorbate per $(\sqrt{5} \times \sqrt{5})R26.6°$ supercell on the $Ti_{3/5}$ coverage is explored. We do so to attain fundamental understanding of water interacting with a highly reduced surface, without the complexity of intermolecular water effects leading to additional electronic structure changes or structural rearrangements. The maximum interaction between a water molecule and the surface occurs at this low coverage.

Figure 1 shows the structure of the bare surface and the range of structures corresponding to reactions 1−5. Adsorption is modeled by saturating one inequivalent binding site ($Ti_A$ or $Ti_B$) at a time. Figure 1b shows the product of reaction 1, in which molecular water interacts with the surface. The $Ti_A$−$O_w$ (water oxygen) bond length is 2.30 Å and makes an angle of 15° relative to the surface normal. The water molecule is tilted with respect to the surface, with one $Ti_A$−$O_w$−H bond angle at 75° (OH pointing down) and the other at 119° (OH pointing horizontally). The H−$O_w$−H angle is 108°. One hydrogen atom of the molecule makes a 1.60 Å hydrogen bond with a surface lattice oxygen. By contrasting the electronic structures of the bare and molecular adsorption configurations, we can conclude that molecular adsorption is a physisorbed state. The projected density of states for the two surfaces (Figure 2a and b) show that the electronic structure of the surface is not perturbed very much by the presence of $H_2O$. The $d_{xz}$ and $d_{yz}$ orbitals of $Ti_A$, however, now become filled, whereas the $d_{z^2}$ orbital moves up in energy and empties. This is an expected electronic response due to repulsion between the water molecule (along *z*) and the nonbonding electron.

Dissociative adsorption reactions 2 and 3 are seen in Figure 1c and d, respectively. The OH would most likely adsorb to a Ti adatom, whereas the H atom would adsorb to an adjacent lattice oxygen or another Ti adatom. Figure 1c shows the $Ti_A$ as the OH binding site while H attaches to the least coordinated lattice O adjacent to $Ti_A$, henceforth referred to as $Ti_A(OH)$-($O_lH$). Figure 1d, on the other hand, shows the H bonded to the nearest $Ti_B$ site, henceforth referred to as $Ti_A(OH)Ti_{B'}H$. $Ti_A(OH)(O_lH)$ is 2.1 kJ/mol $H_2O$ more stable than $Ti_A(OH)$-$Ti_{B'}H$. Given the fact that this is the case, it is very likely that the H atom could diffuse on the surface and access both configurations at finite temperatures (thermal energy: $k_BT$ = 2.5 kJ/mol at 298 K). In $Ti_A(OH)(O_lH)$, $Ti_A$ acts as a Lewis acid and $O_l$ as a Bronsted base. The Ti−$O_w$ bond length is 1.92 Å and the Ti−$O_w$−H angle is 129°. The $O_l$−H bond length is 0.98 Å and is at a 66° angle with respect to the surface normal. By contrast, in the $Ti_A(OH)Ti_{B'}H$ configuration, $Ti_A$ and $Ti_{B'}$ function as reducing species, and both become oxidized. This produces a hydride from a proton of water, which adsorbs to $Ti_{B'}$ (electronic structure discussed below). $Ti_A$ and $Ti_{B'}$ also perform as Lewis acid sites after proton reduction in this case.

$Ti_A(OH)Ti_{B'}H$ also differs from $Ti_A(OH)(O_lH)$ in terms of bond lengths and bond angles. In $Ti_A(OH)Ti_{B'}H$, the $Ti_A$−$O_w$ bond length is 1.85 Å and the $Ti_A$−$O_w$−H angle is 113°. The $Ti_{B'}$−H bond is 1.867 Å and is tilted toward the OH at 23° with respect to the surface normal. The $Ti_A$−$O_w$ bond lengths are in reasonable agreement with a previous quantum chemical calculation of the Ti−OH bond length in the $Ti(OH)_4$ molecule (1.81 Å).[22] Furthermore, various quantum chemical calculations have given a Ti−H bond length of about 1.7 Å for organic Ti hydrides,[23] and DFT-GGA predicted the bond length for the TiH dimer to be 1.8 Å,[24] which are in reasonable agreement with the Ti−H bond length herein.

Comparing the electronic structures of the two dissociative configurations (Figure 2c and d) with the molecular adsorption and bare surface cases, we see that either the occupied $Ti_A$ 3d state(s) changed valence orbital character (remaining occupied) similar to the physisorption case, as in $Ti_A(OH)(O_lH)$, or moved to the conduction band (becoming less occupied), as in $Ti_A(OH)Ti_{B'}H$. It is clear that the electronic population profiles, and therefore the oxidation states, of the Ti adatoms are unchanged in $Ti_A(OH)(O_lH)$. In $Ti_A(OH)Ti_{B'}H$, however,


dx.doi.org/10.1021/jz501635f | J. Phys. Chem. Lett. 2014, 5, 3408−3414

both $Ti_A$ and $Ti_{B'}$ were oxidized, whereas the H from water that moves to $Ti_{B'}$ is greatly reduced. Figure 2e shows the protonic profile of the H on $O_w$ and a hyrdridic electronic profile for H on $Ti_{B'}$, where the two occupied H 1s PDOS peaks (spin up and down, zoomed-in and spin-resolved in Figure 2e) are hybridized with the $Ti_{B'}$ $3d_{z^2}$ orbital. Table 1 shows the calculated Löwdin charges of pertinent surface species for structures found in Figure 1a–d. These charges further illustrate that water may react with the surface in an acid–base type reaction as in $Ti_A(OH)(O_lH)$, where the Löwdin charges on the Ti adatoms remain the same, or in a redox type reaction as in $Ti_A(OH)Ti_{B'}H$, where the Löwdin charges on the Ti adatoms increase. Also shown is the very negative Löwdin charge on H on top of $Ti_{B'}$ (−0.67*e* vs +0.4*e* in protonic H).

Reduced Ti–H species on oxide surfaces are rare but have been observed. A recent study found that Ti–H hydrides were the photoactive species on the defective (via oxygen vacancy) rutile $TiO_2$(110) surface.[25] Various spectroscopic techniques confirmed the existence of the hydride-type species, and DFT calculations identified O vacancies at the O-bridging sites and basal 5-fold coordinated Ti sites (coordinately unsaturated sites) as stable hydride adsorption sites. Notably, the Ti–H species are stable because of excess electrons on the surface due to the oxygen vacancies, which is analogous to our case, in which the nonstoichiometric surface reconstruction is Ti-rich. The existence and stability of these Ti–H species on a reduced $TiO_2$ (110) surface is further supported by scanning tunneling microscopy (STM) and electron stimulated desorption (ESD) studies[26] in which an H atom is shown to form a hydride when it gets trapped at an oxygen vacancy site. Titanium hydrides were also observed in low energy ion scattering (LEIS) measurements of $H_2^+$ ions adsorbing on a highly oxygen deficient $TiO_2$ (110) surface.[27] These studies show an O-vacancy-mediated hydride-type species formation as opposed to being excess-Ti-mediated.

Oxidative adsorption reaction (reactions 4 and 5) products are seen in Figure 1e and f, respectively. They are the oxidized surface structures that result from surface $H_2$ generation and desorption. In the $Ti_A$–OH configuration, the $Ti_A$–$O_w$ bond length is 1.89 Å and the bond is oriented perpendicular to the surface. In $Ti_A$=O, the $Ti_A$–$O_w$ is shorter (1.68 Å). Figure 3a and b show the atomic PDOS of select surface species for $Ti_A$–OH and $Ti_A$–O, respectively. It is clear that the $Ti_A$ in both cases is oxidized, as seen by the absence of significantly occupied 3d orbitals and the increased positive Löwdin charges (Table 1). The calculated charge on $Ti_A$ for $Ti_A$=O is less positive, however, which may seem counterintuitive, but it is due to the very covalent bond between $Ti_A$ and $O_w$. The high energy oxygen 2p peaks (red) located between −2.0 and −4.0 eV in the density of states of $Ti_A$=O (see also Figure 3c) are due to $\sigma$ and $\pi$ bonding between the oxygen and $Ti_A$. The high covalency of the interaction can be seen from the overlapping Ti 3d and O 2p projections in this energy window, wherein the $p_z$ orbital of O overlaps the $3d_{z^2}$ orbital of the $Ti_A$, and the $p_x$ and $p_y$ orbitals of O overlap the $d_{xz}$ and $d_{yz}$ orbitals of the $Ti_A$. This type of surface defect (TiO unit) has been shown to organize into ordered structures on the (001) surface of $BaTiO_3$, producing either a $c(2\times 2)$ or $c(4\times 4)$ reconstruction.[21] Similar calculations have been done for $Ti_B$ as the oxidation site, and their atomic and electronic structures are shown, respectively, in Figures S1 and S2 of the Supporting Information, showing similar properties.

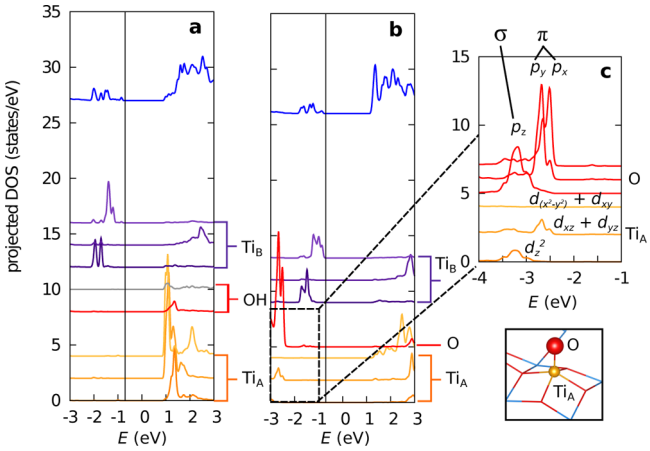


**Figure 3.** Electronic PDOS of the oxidative adsorption products of a water molecule on the $(\sqrt{5} \times \sqrt{5})R26.6°$ reconstruction.(a) Oxidative adsorption with surface OH as the product and (b) with surface O as the product. For Ti adatoms (A and B), the DOS contribution is resolved to show orbital types: $d_{z^2}$, $d_{xz}$ + $d_{yz}$ and $d_{x^2-y^2}$ + $d_{xy}$ from bottom to top. See Figure 1e and f for the corresponding atomic structures. (c) orbital resolved projection of the O adsorbates 2p orbitals in (b) where the $p_z$ orbital overlaps with the $d_{z^2}$ ($Ti_A$–O $\sigma$ bonding), and $p_x$ and $p_y$ orbital overlap with the $d_{xz}$ and $d_{yz}$ orbitals ($Ti_A$–O $\pi$ bonding). Lower panel in (c) shows the surface $Ti_A$–O structure (see Figure 1 for legend). For the PDOS, the valence band maxima were aligned, which are set to −0.7 eV[20] for ease of comparison.

To produce either $Ti_A$–OH or $Ti_A$–O, a mechanism to stably produce and desorb $H_2$ from the surface must be in operation. Figure 4a and b illustrate stepwise mechanisms for how reactions 6 and 7 may occur to produce $H_2$ after dissociative adsorption of $H_2O$ on the surface. Figure 4a shows a reaction leading to surface hydroxyls and liberation of $H_2$(gas). A proton from an $O_l$ site (coming from $Ti_A(OH)(O_lH)$) may hop to another lattice O site adjacent to a $Ti_{B'}$ with a hydride adsorbed. Then a nucleophilic attack onto the proton from the hydride produces $H_2$. Figure 4b, on the other hand, shows production of $Ti_A$=O and $H_2$(gas), where starting from a $Ti_A(OH)Ti_{B'}H$ configuration, a nucleophilic attack by the hydride onto the proton of the hydroxyl produces $H_2$.

The mechanism of water reduction with concomitant release of hydrogen gas has been explored extensively in metal and metal oxide clusters[28−32] where active sites are more available and accessible. Indeed, surfaces have a tendency to restrict access to active sites due to the rigidity of the underlying structures and reduced dimensionality of the architecture.[33,34] We have shown, however, that on the Ti covered $TiO_2$ surface of $BaTiO_3$, the multiple active sites are sufficiently exposed to alleviate structural restrictions in catalyzing reactions requiring multiple reaction sites.

The energetics for hydrogen production as outlined in Figure 4 (reactions 6 and 7 in Table 2) is comparable to that of known $H_2$ catalysts. In Figure 4a, the reaction energy can be approximated by the energies of twice reaction 4 minus the sum of reactions 2 and 3, yielding an energy cost of +67 kJ/mol. In Figure 4b, the reaction energy is approximated by the energy of reaction 5 minus the energy of reaction 3, yielding an energy cost of +54 kJ/mol. For the former reaction, the $Ti_B$ centered reaction is found to be exothermic,−25 kJ/mol, whereas for the latter reaction, the $Ti_B$ centered reaction has a higher barrier of +77 kJ/mol (see Table 2). These are less than


dx.doi.org/10.1021/jz501635f | J. Phys. Chem. Lett. 2014, 5, 3408−3414

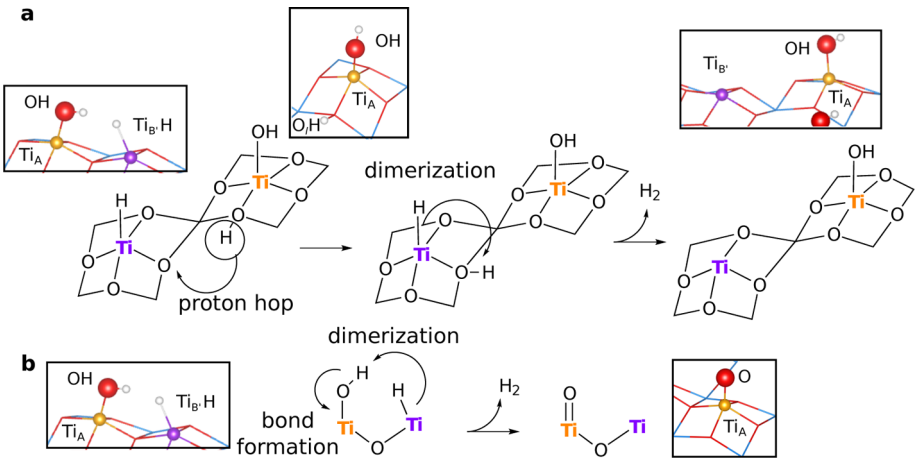


**Figure 4.** Hydrogen producing reaction scheme from dissociated water. The hydride at the $Ti_{B'}$ site can react (a) with a proton that hops to an adjacent lattice O ($O_l$) site from an $O_l$ site associated with an OH on a $Ti_A$ site, reaction 6, or (b) directly with the proton from an OH on the adjacent $Ti_A$ site, reaction 7.

**Table 2. Reaction Energetics of the Different Water Adsorption Types for when $Ti_A$ and $Ti_B$ Are the Main Reaction Sites**[a]

| reaction | $\Delta E$ (DFT-GGA+$U$ [4.9 eV]) [kJ/mol] | |
|---|---|---|
| | $Ti_A$ | $Ti_B$ |
| (1) $Ti_{A/B} + H_2O \rightarrow Ti_{A/B}{-}OH_2$ | −61.8 | −62.3 |
| (2) $Ti_{A/B} + O_{lattice} + H_2O \rightarrow Ti_{A/B}{-}OH + O_{lattice}H$ | −129.7 | −106.7 |
| (3) $Ti_{A/B} + Ti_{B/A} + H_2O \rightarrow Ti_{A/B}{-}OH + Ti_{B/A}H$ | −127.6 | −131.9 |
| (4) $Ti_{A/B} + H_2O \rightarrow Ti_{A/B}{-}OH + \frac{1}{2}H_2$ | −95.0 | −131.7 |
| (5) $Ti_{A/B} + H_2O \rightarrow Ti_{A/B} = O + H_2$ | −73.6 | −55.3 |
| (6) $Ti_{B/A}H + O_{lattice}H \rightarrow Ti_{B/A} + O_{lattice} + H_2$ | +67.3 | −24.8 |
| (7) $Ti_{A/B}{-}OH + Ti_{B/A}H \rightarrow Ti_{A/B} = O + H_2$ | +54.0 | +76.6 |

[a]The differences between the reaction energies of the two sites indicate that they are chemically distinct from each other, especially in the proton transfer, (2) into (3), and toward oxidation, which includes reactions (4) and (5).

or comparable to the calculated barriers for the rate-limiting dimerization of H to $H_2$ on known $H_2$ producing catalysts, such as Pt (111), +73 kJ/mol, Ni (111), +103.2 kJ/mol, and $Ni_2P$ (001), +43.4 kJ/mol, in low surface coverage.[35]

The catalytic efficiency can be linearly correlated to certain thermodynamic parameters, known as descriptors (e.g., adsorption energies), which are effective in finding candidate catalysts.[35−40] However, further exploration into the effect of adsorbate concentration and environmental chemical constraints on the barriers will enhance the understanding of this class of catalytic surfaces in realistic operational conditions. We have clearly demonstrated, nonetheless, the ability of the surface to stabilize a hydride on the surface essential for $H_2$ production or hydride-dependent chemistries, for example, the water−gas shift reaction.

Oxidation of the surface with water leads to production of hydrides and ultimately to $H_2$ gas (water reduction). We explore a pathway of $H_2$ production by explicitly showing a possible path for hydride formation from water. Furthermore, we find that the direct reaction of $H_2O$ with a Ti adatom does not spontaneously lead to a $H_2$ bond formation between the hydrogen atoms of the incoming water molecule. Therefore, we propose an initial dissociative adsorption state where OH is adsorbed on a Ti adatom, whereas the H bonds with the least coordinated surface O or another Ti adatom. In the former case, the H carries a net positive charge, whereas in the latter case H carries a net negative charge. The reaction of an electron-rich and an electron-deficient H then forms an $H_2$ gas molecule, ultimately oxidizing the surface Ti adatoms.

Water reduction is of great interest because it is a method to generate hydrogen gas, which is an attractive alternative fuel resulting in no pollutants. Water reduction often is conducted in the presence of a catalyst, as in the electrocatalytic hydrogen production from water: $2H_2O + 2e^- \rightarrow H_2 + 2OH^-$,[35,41] the water−gas shift reaction: $CO + H_2O \rightarrow H_2 + CO_2$,[42,43] and the steam reforming of ethanol: $C_2H_5OH + 3H_2O \rightarrow 2CO_2 + 6H_2$.[42] In the first reaction, Pt, $Ni_2P$,[35,41] and $MoS_2$[44−46] have been shown to be good catalysts, whereas the latter two reactions are commonly catalyzed by a combination of a metal and a metal oxide, such as $Au/CeO_2$,[47] $Ni/CeO_2$,[42] and $Cu/ZnO$.[43] In these reactions, hydrides are important reaction intermediates. It is plausible that the $(\sqrt{5} \times \sqrt{5})R26.6°$ reconstruction of $BaTiO_3$ (001) could catalyze a hydrogen generating reaction without the need for a metal cocatalyst, as there is an equilibrium between the two dissociative adsorption states as shown earlier. The equilibrium, moreover, is characterized by an energy barrier that can be surmounted via thermal energy. In the reduction of water, eventual protonation of Ti−OH and Ti═O and electroreduction of the Ti sites would lead to a reversible water desorption, leaving


dx.doi.org/10.1021/jz501635f | J. Phys. Chem. Lett. 2014, 5, 3408−3414

behind the hydrides and, thus, leading to H-enrichment of the surface. In the water−gas shift and steam reforming, CO or other small, reduced hydrocarbons may be used to sequester the O species left behind from $H_2$ formation which will then re-expose the reduced Ti.

## COMPUTATIONAL METHODS

The spin-polarized, effective *U*-corrected[48] density functional theory calculations were performed with the Quantum ESPRESSO DFT package,[49] with a 50 Ry plane-wave cutoff and the PBE-GGA functional.[50] The *U* correction was applied to the Ti 3d states ($U$ = 4.9 eV)[20] and the core states of all elements were described using norm-conserving pseudopotentials generated with the OPIUM code.[51] A 4 × 4 × 1 Monkhorst−Pack[52] k-point mesh was used for relaxation calculations and a 10 × 10 × 1 mesh was used for the density of states calculations. The surface calculations were performed using a slab model containing six atomic layers, with the in-plane periodicity of the supercell fixed at 4.00 $\sqrt{5}$ Å. During relaxation calculations, the atomic positions of the top three layers, adatoms, and adsorbates were relaxed until the forces on atoms were less than 0.01 eV/Å in all directions, whereas the bottom three layers were fixed to a cubic structure. Approximately 20 Å of vacuum separate the slabs in order to prevent artificial electric field interactions between images. A molecule in a box, where images are separated by a vacuum, was used to simulate the $H_2$ and $H_2O$ molecules. Calculations were then performed at the Γ-point of the Brillouin zone.

## ASSOCIATED CONTENT

### Supporting Information

Atomic and electronic structures of $Ti_B$ centered water adsorption reactions. Layer-by-layer PDOS for $Ti_A$ centered reactions. This material is available free of charge via the Internet at http://pubs.acs.org/.

## AUTHOR INFORMATION

### Corresponding Author

*E-mail: rappe@sas.upenn.edu.

### Notes

The authors declare no competing financial interest.

## ACKNOWLEDGMENTS

N.Z.K. was supported by the National Science Foundation, under Grant Number DMR-1124696, and by the Roy & Diana Vagelos Scholars Program in the Molecular Life Sciences. J.M.P.M. was supported by the National Science Foundation, under Grant Number CMMI-1334241. A.M.R. was supported by the Department of Energy Office of Basic Energy Sciences, under grant number DE-FG02-07ER15920. Computational support was provided by the High-Performance Computing Modernization Office of the Department of Defense and the National Energy Research Scientific Computing Center.

## REFERENCES

(1) Hodgson, A.; Haq, S. Water Adsorption and the Wetting of Metal Surfaces. *Surf. Sci. Rep.* **2009**, *64*, 381−451.

(2) Carrasco, J.; Hodgson, A.; Michaelides, A. A Molecular Perspective of Water at Metal Interfaces. *Nat. Mater.* **2012**, *11*, 667−674.

(3) Limmer, D. T.; Willard, A. P.; Madden, P.; Chandler, D. Hydration of Metal Surfaces Can Be Dynamically Heterogeneous and Hydrophobic. *Proc. Natl. Acad. Sci. U.S.A.* **2013**, *110*, 4200−4205.

(4) Henderson, M. A. The Interaction of Water with Solid Surfaces: Fundamental Aspects Revisited. *Surf. Sci. Rep.* **2002**, *46*, 1−308.

(5) Calatayud, M.; Markovits, A.; Menetrey, M.; Mguig, B.; Minot, C. Adsorption on Perfect and Reduced Surfaces of Metal Oxides. *Catal. Today* **2003**, *85*, 125−143.

(6) Shin, J.; Nascimento, V. B.; Geneste, G.; Rundgren, J.; Plummer, E. W.; Dkhil, B.; Kalinin, S. V.; Baddorf, A. P. Atomistic Screening Mechanism of Ferroelectric Surfaces: An In Situ Study of the Polar Phase in Ultrathin $BaTiO_3$ Films Exposed to $H_2O$. *Nano Lett.* **2009**, *9*, 3720−3725.

(7) Garra, J.; Vohs, J.; Bonnell, D. A. The Effect of Ferroelectric Polarization on the Interaction of Water and Methanol with the Surface of $LiNbO_3$(0001). *Surf. Sci.* **2009**, *603*, 1106−14.

(8) Geneste, G.; Dkhil, B. Adsorption and Dissociation of $H_2O$ on In-Plane-Polarized $BaTiO_3$(001) Surfaces and their Relation to Ferroelectricity. *Phys. Rev. B* **2009**, *79*, 235420.

(9) Au, K.; Li, D. F.; Chan, N. Y.; Dai, J. Y. Polar Liquid Molecule Induced Transport Property Modulation at $LaAlO_3/SrTiO_3$ Heterointerface. *Adv. Mater.* **2012**, *24*, 2598−2602.

(10) Evarestov, R.; Bandura, A.; Alexandrov, V. Adsorption of Water on (001) Surface of $SrTiO_3$ and $SrZrO_3$ Cubic Perovskites: Hybrid HF-DFT {LCAO} Calculations. *Surf. Sci.* **2007**, *601*, 1844−1856.

(11) Baniecki, J. D.; Ishii, M.; Kurihara, K.; Yamanaka, K.; Yano, T.; Shinozaki, K.; Imada, T.; Kobayashi, Y. Chemisorption of Water and Carbon Dioxide on Nanostructured $BaTiO_3$-$SrTiO_3$(001) Surfaces. *J. Appl. Phys.* **2009**, *106*, 054109.

(12) Guhl, H.; Miller, W.; Reuter, K. Water Adsorption and Dissociation on $SrTiO_3$(001) Revisited: A Density Functional Theory Study. *Phys. Rev. B* **2010**, *81*, 155455.

(13) Becerra-Toledo, A.; Castell, M.; Marks, L. Water Adsorption on $SrTiO_3$(001): I. Experimental and Simulated STM. *Surf. Sci.* **2012**, *606*, 762−765.

(14) Becerra-Toledo, A.; Enterkin, J.; Kienzle, D.; Marks, L. Water adsorption on $SrTiO_3$(001): II. Water, water, everywhere. *Surf. Sci.* **2012**, *606*, 791−802.

(15) Wang, Z.; Hao, X.; Gerhold, S.; Novotny, Z.; Franchini, C.; McDermott, E.; Schulte, K.; Schmid, M.; Diebold, U. Water Adsorption at the Tetrahedral Titania Surface Layer of $SrTiO_3$(110)-(4 × 1). *J. Phys. Chem. C* **2013**, *117*, 26060−26069.

(16) Li, W.; Liu, S.; Wang, S.; Guo, Q.; Guo, J. The Roles of Reduced Ti Cations and Oxygen Vacancies in Water Adsorption and Dissociation on $SrTiO_3$(110). *J. Phys. Chem. C* **2014**, *118*, 2469−2474.

(17) Wang, J. L.; Gaillard, F.; Pancotti, A.; Gautier, B.; Niu, G.; Vilquin, B.; Pillard, V.; Rodrigues, G. L. M. P.; Barrett, N. Chemistry and Atomic Distortion at the Surface of an Epitaxial $BaTiO_3$ Thin Film after Dissociative Adsorption of Water. *J. Phys. Chem. C* **2012**, *116*, 21802−21809.

(18) Spanier, J. E.; Kolpak, A. M.; Urban, J. J.; Grinberg, I.; Ouyang, L.; Yun, W. S.; Rappe, A. M.; Park, H. Ferroelectric Phase Transition in Individual Single-Crystalline $BaTiO_3$ Nanowires. *Nano Lett.* **2006**, *6*, 735−9.

(19) Kolpak, A. M.; Li, D.; Shao, R.; Rappe, A. M.; Bonnell, D. A. Evolution of the Structure and Thermodynamic Stability of the $BaTiO_3$(001) Surface. *Phys. Rev. Lett.* **2008**, *101*, 036102.

(20) Martirez, J. M. P.; Morales, E. H.; Saidi, W. A.; Bonnell, D. A.; Rappe, A. M. Atomic and Electronic Structure of the $BaTiO_3$(001)-($\sqrt{5}$ × $\sqrt{5}$)R26.6° Surface Reconstruction. *Phys. Rev. Lett.* **2012**, *109*, 256802.

(21) Morales, E. H.; Martirez, J. M. P.; Saidi, W. A.; Rappe, A. M.; Bonnell, D. A. Coexisting Surface Phases and Coherent One-Dimensional Interfaces on $BaTiO_3$(001). *ACS Nano* **2014**, *8*, 4465−4473.

(22) Wang, T.-H.; Navarrete-Lopez, A. M.; Li, S.; Dixon, D. A.; Gole, J. L. Hydrolysis of $TiCl_4$: Initial Steps in the Production of $TiO_2$. *J. Phys. Chem. A* **2010**, *114*, 7561−7570.

(23) Andrews, L.; Cho, H.-G.; Wang, X. Reactions of Methane with Titanium Atoms: $CH_3TiH$, $CH_2TiH_2$, Agostic Bonding, and $(CH_3)_2TiH_2$. *Inorg. Chem.* **2005**, *44*, 4834−4842.

(24) Venkataramanan, N. S.; Sahara, R.; Mizuseki, H.; Kawazoe, Y. Titanium-Doped Nickel Clusters $TiNi_n$ ($n$ = 1−12): Geometry, Electronic, Magnetic, and Hydrogen Adsorption Properties. *J. Phys. Chem. A* **2010**, *114*, 5049−5057.
(25) Wu, Z.; Zhang, W.; Xiong, F.; Yuan, Q.; Jin, Y.; Yang, J.; Huang, W. Active Hydrogen Species on $TiO_2$ for Photocatalytic $H_2$ Production. *Phys. Chem. Chem. Phys.* **2014**, *16*, 7051−7057.
(26) Suzuki, S.; Fukui, K.-i.; Onishi, H.; Iwasawa, Y. Hydrogen Adatoms on $TiO_2$(110)-(1 × 1) Characterized by Scanning Tunneling Microscopy and Electron Stimulated Desorption. *Phys. Rev. Lett.* **2000**, *84*, 2156−2159.
(27) Pan, J.; Maschhoff, B. L.; Diebold, U.; Madey, T. E. Interaction of Water, Oxygen, and Hydrogen with $TiO_2$(110) Surfaces Having Different Defect Densities. *J. Vac. Sci. Technol., A* **1992**, *10*, 2470−2476.
(28) Mayhall, N. J.; Rothgeb, D. W.; Hossain, E.; Jarrold, C. C.; Raghavachari, K. Water Reactivity with Tungsten Oxides: $H_2$ Production and Kinetic Traps. *J. Chem. Phys.* **2009**, *131*, 144302.
(29) Rothgeb, D. W.; Hossain, E.; Mayhall, N. J.; Raghavachari, K.; Jarrold, C. C. Termination of the $W_2O_y + H_2O/D_2O \rightarrow W_2O_{y+1} + H_2/D_2$ Sequential Oxidation Reaction: An Exploration of Kinetic Versus Thermodynamic Effects. *J. Chem. Phys.* **2009**, *131*, 144306.
(30) Li, X.-N.; Xu, B.; Ding, X.-L.; He, S.-G. Interaction of Vanadium Oxide Cluster Anions with Water: An Experimental and Theoretical Study on Reactivity and Mechanism. *Dalton Trans.* **2012**, *41*, 5562−5570.
(31) Reber, A. C.; Khanna, S. N.; Roach, P. J.; Woodward, W. H.; Castleman, A. W., Jr. Reactivity of Aluminum Cluster Anions with Water: Origins of Reactivity and Mechanisms for $H_2$ Release. *J. Phys. Chem. A* **2010**, *114*, 6071−6081.
(32) Fang, Z.; Dixon, D. A. Computational Study of $H_2$ and $O_2$ Production from Water Splitting by Small $(MO_2)_n$ Clusters (M = Ti, Zr, Hf). *J. Phys. Chem. A* **2013**, *117*, 3539−3555.
(33) Hutchings, G. J. Metal-Cluster Catalysts: Access granted. *Nat. Chem.* **2010**, *2*, 1005−1006.
(34) Huang, W. Crystal Plane-Dependent Surface Reactivity and Catalytic Property of Oxide Catalysts Studied with Oxide Nanocrystal Model Catalysts. *Top. Catal.* **2013**, *56*, 1363−1376.
(35) Liu, P.; Rodriguez, J. A. Catalysts for Hydrogen Evolution from the [NiFe] Hydrogenase to the $Ni_2P$(001) Surface: The Importance of Ensemble Effect. *J. Am. Chem. Soc.* **2005**, *127*, 14871−14878.
(36) Nørskov, J. K.; Bligaard, T.; Rossmeisl, J.; Christensen, C. H. Towards the Computational Design of Solid Catalysts. *Nat. Chem.* **2009**, *1*, 37−46.
(37) Nørskov, J. K.; Rossmeisl, J.; Logadottir, A.; Lindqvist, L.; Kitchin, J. R.; Bligaard, T.; Jónsson, H. Origin of the Overpotential for Oxygen Reduction at a Fuel-Cell Cathode. *J. Phys. Chem. B* **2004**, *108*, 17886−17892.
(38) Peterson, A. A.; Nørskov, J. K. Activity Descriptors for $CO_2$ Electroreduction to Methane on Transition-Metal Catalysts. *J. Phys. Chem. Lett.* **2012**, *3*, 251−258.
(39) Man, I. C.; Su, H.-Y.; Calle-Vallejo, F.; Hansen, H. A.; Martínez, J. I.; Inoglu, N. G.; Kitchin, J.; Jaramillo, T. F.; Nørskov, J. K.; Rossmeisl, J. Universality in Oxygen Evolution Electrocatalysis on Oxide Surfaces. *ChemCatChem.* **2011**, *3*, 1159−1165.
(40) Studt, F.; Sharafutdinov, I.; Abild-Pedersen, F.; Elkjaer, C. F.; Hummelshoj, J. S.; Dahl, S.; Chorkendorff, I.; Nørskov, J. K. Discovery of a Ni-Ga Catalyst for Carbon Dioxide Reduction to Methanol. *Nat. Chem.* **2014**, *6*, 320−324.
(41) Popczun, E. J.; McKone, J. R.; Read, C. G.; Biacchi, A. J.; Wiltrout, A. M.; Lewis, N. S.; Schaak, R. E. Nanostructured Nickel Phosphide as an Electrocatalyst for the Hydrogen Evolution Reaction. *J. Am. Chem. Soc.* **2013**, *135*, 9267−9270.
(42) Senanayake, S.; Rodriguez, J.; Stacchiola, D. Electronic Metal-Support Interactions and the Production of Hydrogen Through the Water-Gas Shift Reaction and Ethanol Steam Reforming: Fundamental Studies with Well-Defined Model Catalysts. *Top. Catal.* **2013**, *56*, 1488−1498.
(43) Rodriguez, J. A.; Hanson, J. C.; Stacchiola, D.; Senanayake, S. D. In Situ/Operando Studies for the Production of Hydrogen through the Water-Gas Shift on Metal Oxide Catalysts. *Phys. Chem. Chem. Phys.* **2013**, *15*, 12004−12025.
(44) Karunadasa, H. I.; Montalvo, E.; Sun, Y.; Majda, M.; Long, J. R.; Chang, C. J. A Molecular $MoS_2$ Edge Site Mimic for Catalytic Hydrogen Generation. *Science* **2012**, *335*, 698−702.
(45) Li, Y.; Wang, H.; Xie, L.; Liang, Y.; Hong, G.; Dai, H. $MoS_2$ Nanoparticles Grown on Graphene: An Advanced Catalyst for the Hydrogen Evolution Reaction. *J. Am. Chem. Soc.* **2011**, *133*, 7296−7299.
(46) Jaramillo, T. F.; Jørgensen, K. P.; Bonde, J.; Nielsen, J. H.; Horch, S.; Chorkendorff, I. Identification of Active Edge Sites for Electrochemical $H_2$ Evolution from $MoS_2$ Nanocatalysts. *Science* **2007**, *317*, 100−102.
(47) Song, W.; Hensen, E. J. M. Mechanistic Aspects of the Water-Gas Shift Reaction on Isolated and Clustered Au Atoms on $CeO_2$(110): A Density Functional Theory Study. *ACS Catal.* **2014**, *4*, 1885−1892.
(48) Cococcioni, M.; de Gironcoli, S. Linear Response Approach to the Calculation of the Effective Interaction Parameters in the LDA + $U$ Method. *Phys. Rev. B* **2005**, *71*, 035105.
(49) Giannozzi, P.; et al. Quantum ESPRESSO: A Modular and Open-Source Software Project for Quantum Simulations of Materials. *J. Phys.: Condens. Matter* **2009**, *21*, 395502.
(50) Perdew, J. P.; Burke, K.; Ernzerhof, M. Generalized Gradient Approximation Made Simple. *Phys. Rev. Lett.* **1996**, *77*, 3865−3868.
(51) Opium—Pseudopotential Generation Project. http://opium.sourceforge.net.
(52) Monkhorst, H. J.; Pack, J. D. Special Points for Brillouin-Zone Integrations. *Phys. Rev. B* **1976**, *13*, 5188−5192.